Published in final edited form as:
Contrast Media Mol Imaging. 2015 January ; 10(1): 51–58. doi:10.1002/cmmi.1604.

Lanthanide ion (III) complexes of 1,4,7,10-tetraazacyclododecane-1,4,7,10-tetraaminophosphonate (DOTA-4AmP^{8-}) for dual biosensing of pH with CEST (chemical exchange saturation transfer) and BIRDS (biosensor imaging of redundant deviation in shifts)

Yuegao Huang[a,b], **Daniel Coman**[a,b,c], **Meser M. Ali**[d], and **Fahmeed Hyder**[a,b,c,e,*]

[a] Department of Diagnostic Radiology, Yale University, New Haven, CT 06520, USA

[b] Magnetic Resonance Research Center (MRRC), Yale University, New Haven, CT 06520, USA

[c] Core Center for Quantitative Neuroscience with Magnetic Resonance (QNMR), Yale University, New Haven, CT 06520, USA

[d] Department of Neurology, Henry Ford Hospital, Detroit, MI 48202, USA

[e] Department of Biomedical Engineering, Yale University, New Haven, CT 06520, USA

Abstract

Relaxivity based magnetic resonance of phosphonated ligands chelated with gadolinium (Gd^{3+}) shows promise for pH imaging. However instead of monitoring the paramagnetic effect of lanthanide complexes on the relaxivity of water protons, biosensor (or molecular) imaging with magnetic resonance is also possible by detecting either the non-exchangeable or the exchangeable protons on the lanthanide complexes themselves. The non-exchangeable protons (e.g., $–CH_x$, where $3 \geq x \geq 1$) are detected using a three-dimensional chemical shift imaging method called Biosensor Imaging of Redundant Deviation in Shifts (BIRDS), whereas the exchangeable protons (e.g., –OH or $–NH_y$, where $2 \geq y \geq 1$) are measured with Chemical Exchange Saturation Transfer (CEST) contrast. Here we tested the feasibility of BIRDS and CEST for pH imaging of 1,4,7,10-tetraazacyclododecane-1,4,7,10-tetraaminophosphonate (DOTA-4AmP^{8-}) chelated with thulium (Tm^{3+}) and ytterbium (Yb^{3+}). BIRDS and CEST experiments show that both complexes are responsive to pH and temperature changes. Higher pH and temperature sensitivities are obtained with BIRDS for either complex when using the chemical shift difference between two proton resonances vs. using the chemical shift of a single proton resonance, thereby eliminating the need to use water resonance as reference. While CEST contrast for both agents is linearly dependent on pH within a relatively large range (i.e., 6.3-7.9), much stronger CEST contrast is obtained with YbDOTA-4AmP^{5-} than with TmDOTA-4AmP^{5-}. In addition, we demonstrate the prospect of using BIRDS to calibrate CEST as new platform for quantitative pH imaging.

* Correspondence to: F. Hyder, N135 TAC (MRRC), 300 Cedar Street, Yale University, New Haven, CT 06520, USA. fahmeed.hyder@yale.edu.

1. INTRODUCTION

Accurate measurement of pH is an active topic in molecular biosensing with magnetic resonance (MR) methods (1,2). Several MR methods, both imaging (MRI) and spectroscopy (MRS), are available to monitor tissue pH (3). For example, a popular MRI approach to assess the pH is based on measuring the relaxivity of bulk water protons using a phosphonated ligand – 1,4,7,10-tetraazacyclododecane-1,4,7,10-tetraaminophosphonate (DOTA-4AmP^{8-}) – chelated with lanthanide ions (Ln^{3+}) (4-6). These relaxivity-based studies for in vivo pH scans have successfully designed protocols to administer a pH-dependent contrast agent containing gadolinium (Gd^{3+}) (e.g., Gd-DOTA-4AmP^{5-}) in conjunction with another pH-insensitive contrast agent containing dysprosium (Dy^{3+}) (e.g., Dy-DOTP^{5-}) (5,6). The pH-insensitive agent is used for concentration reference of the pH-sensitive agent whose relaxivity is pH-dependent. While relaxivity-based measurements detect the effect of the Gd^{3+} complexes on the water protons, MRS methods measure pH using chemical shifts of endogenous and/or exogenous complexes containing pH-sensitive nuclei (e.g., hyperpolarized ^{13}C, ^{1}H, ^{31}P, and ^{19}F) (7-10). Although these methods show great potential for pH imaging, in vivo applications are somewhat limited due to concerns about low spatial resolution, spectral overlapping, and need for state-of-the-art hardware for hyperpolarized technology.

pH can also be measured using signals emanating from either the non-exchangeable or exchangeable protons of the lanthanide complexes (11-13). The exchangeable protons (e.g., –OH or –NH$_y$, where y=1 or 2) are observed with an MRI method called Chemical Exchange Saturation Transfer (CEST), whereas the non-exchangeable protons (e.g., –CH$_x$, where x=1,2 or 3) are detected with MRS or for imaging using a three-dimensional chemical shift imaging method called Biosensor Imaging of Redundant Deviation in Shifts (BIRDS). Balaban and coworkers demonstrated the feasibility for pH imaging with diamagnetic CEST (DIACEST) complexes that contain amine or hydroxyl protons (14-16). They showed that a change in the bulk water pool is observed (i.e., MRI contrast) when the pool of diamagnetic protons is saturated with a selective radio frequency (RF) pulse of low amplitude. Tissue pH can also be evaluated using amide signals from endogenous macromolecules via amide proton transfer, which is a variant of DIACEST mechanism (17). However DIACEST methods are susceptible to direct saturation of water because the chemical shift separation between the pools of diamagnetic exchangeable protons and bulk water protons is rather small (i.e., 1-2 ppm). To circumvent this issue with DIACEST, pH-sensitive paramagnetic CEST (PARACEST) complexes have been developed, which feature a much larger chemical shift separation (i.e., >10 ppm), thereby reducing the concerns about direct water saturation (18).

Recently it was also reported that pH mapping with BIRDS is possible with paramagnetic phosphonate complexes (e.g., TmDOTP^{5-}) (13). In this method, chemical shifts of non-exchangeable protons are paramagnetically shifted due to their close proximity to the Tm^{3+} ion, where the phosphonate groups on the pendant arms are responsible for the pH sensing. Protonation of the phosphonate groups affects the molecular structure of the complex and thus the chemical shifts of the protons on the complex backbone shift in response to pH changes (19). BIRDS of TmDOTP^{5-} can be used for simultaneous temperature and pH

measurements (13). However, no CEST effect is observed in $TmDOTP^{5-}$, possibly because of lacking exchangeable protons (e.g., amide and bound water protons).

Thus we hypothesized that molecules which contain phosphonate groups, similar to $TmDOTP^{5-}$, but which also have amide protons available for proton exchange (detectable with CEST) can be used for dual BIRDS and CEST pH sensing. However, there are other pH reporting molecules, such as DOTA-tetraamide ligands which lack phosphonate groups but can provide pH sensing using CEST (20). Thus, we propose to use the $DOTA\text{-}4AmP^{8-}$ chelate, which contains non-exchangeable, exchangeable protons, and phosphonate groups, to investigate its pH sensing capabilities when chelated with thulium (Tm^{3+}) and ytterbium (Yb^{3+}), using both BIRDS and CEST detection schemes.

2. RESULTS and DISCUSSION

The synthesis of $DOTA\text{-}4AmP^{8-}$ and chelation with lanthanide ions like Tm^{3+} and Yb^{3+} (Figure 1A) were described previously (4,21). The ^{1}H spectra of both complexes show characteristic hyperfine-shifted resonances and their assignments were made according to a previous report (Figure 1B and 1C) (18). Compared to the resonances of Yb-$DOTA\text{-}4AmP^{5-}$, proton resonances of Tm-$DOTA\text{-}4AmP^{5-}$ are shifted farther away from the water resonance. The exchangeable amide protons resonate at ~50 ppm for Tm-$DOTA\text{-}4AmP^{5-}$ at 35 °C, but are not observable for Yb-$DOTA\text{-}4AmP^{5-}$, suggesting that its exchange rate is beyond the observable detection limit.

A series of 10 mM Tm-$DOTA\text{-}4AmP^{5-}$ or Yb-$DOTA\text{-}4AmP^{5-}$ samples at different pH (6.30-7.90) in 90%/10% H_2O/D_2O phosphate buffer were prepared and studied. BIRDS temperature and pH calibration was performed on all proton resonances at various temperatures in the range of 25-40 °C. Temperature and pH dependencies of chemical shifts are depicted in the forms of 3D surface plots (Supplementary Figures 1 and 2) and fitted with a second-order polynomial dependence according to the model

$$\delta = \mathrm{a} + \mathrm{b} \cdot pH + \mathrm{c} \cdot \mathrm{T} + \mathrm{d} \cdot pH^2 + \mathrm{e} \cdot \mathrm{T}^2 + \mathrm{f} \cdot pH \cdot \mathrm{T} \quad (1)$$

where δ is the chemical shift of a non-exchangeable proton on the probe, T and pH are the respective temperature and pH of the sample, and the coefficients a-f are determined from the fit. The fitted coefficients for each proton resonance for Tm-$DOTA\text{-}4AmP^{5-}$ and Yb-$DOTA\text{-}4AmP^{5-}$are outlined in Supplementary Tables 1 and 2, respectively. We choose a second-order polynomial to fit our data because the results show a non-linear dependence for which a second-order polynomial is one of the simplest equations that can describe the chemical shift dependence on temperature and pH.

Regarding pH sensing by MRS with BIRDS, almost all chemical shifts in both complexes are pH sensitive (Table 1). The only pH insensitive proton resonances are H3 and H7 in Yb-$DOTA\text{-}4AmP^{5-}$, with pH sensitivities less than 0.03 ppm/pH unit. The pH sensitivities are different for each resonance. The most pH sensitive resonance in Tm-$DOTA\text{-}4AmP^{5-}$ is H8 (-4.0±0.2 ppm/pH unit at 35 °C) and the least sensitive is H7 (0.24±0.04 ppm/pH unit at 35 °C). The pH sensitivity for any given proton resonance in Yb-$DOTA\text{-}4AmP^{5-}$ (0 to 1.68 ppm/pH unit) is smaller than the corresponding resonance in Tm-$DOTA\text{-}4AmP^{5-}$. The most

sensitive resonance in Yb-DOTA-4AmP^{5-} is also H8 (i.e., -1.68±0.03 ppm/pH unit at 35 °C), similar to Tm-DOTA-4AmP^{5-}.

The chemical shifts of proton resonances in both Tm-DOTA-4AmP^{5-} and Yb-DOTA-4AmP^{5-}are also sensitive to temperature, as observed previously for TmDOTP^{5-} (12,13). The resonances with the highest temperature sensitivity are H4 in both Tm-DOTA-4AmP^{5-} (-1.49 ± 0.03 ppm/°C at pH 7.50) and Yb-DOTA-4AmP^{5-} (-0.52 ± 0.01 ppm/°C at pH 7.48) (Table 1). However H4, H1, and H5 of Tm-DOTA-4AmP^{5-} have wider linewidths (800 to 1400 Hz), indicating that they have shorter transverse relaxation times (T_2 values ranging from 200 to 400 μs). Very short T_2 values would not be favorable for BIRDS detection scheme because the signal would decay too fast (within few hundred microseconds) requiring the use of a very fast CSI method. For example, a fast CSI method (22) involving a very short excitation pulse (200 μs) followed by 3D phase encoding (200 μs) results in a decrease (during the pulse and phase encoding) to about 14 to 37% of the initial intensity, for signals with T_2 between 200 and 400 μs. Thus these three protons are not good candidates for the current BIRDS detection scheme. Therefore, CSI sequences involving ultrashort TE detection schemes (23,24) should be considered to allow detection of resonances with short T_2.

Higher sensitivity in pH and/or temperature measurement can be obtained when chemical shifts of two resonances are used as suggested previously (25-27). Zuo et al first demonstrated that higher temperature accuracy is possible by taking the difference in chemical shifts between two resonances of proton (or other nuclei) in TmDOTP^{5-} that are shifted in different directions upon temperature changes. Using the same approach, in this work, we show much higher pH sensitivity for Tm-DOTA-4AmP^{5-} by combining the two most pH sensitive proton resonances. In Tm-DOTA-4AmP^{5-}, H6 and H8 are the two most pH sensitive proton resonances and their chemical shifts move in opposite directions in response to pH change. Hence the chemical shift difference between these two proton resonances improves the pH sensitivity to 5.2±0.2 ppm/pH unit at 35 °C (Figure 2, Table 1). The enhanced pH sensitivity for Tm-DOTA-4AmP^{5-} is better than those recorded with TmDOTP^{5-} (≤ 4.2 ppm/pH unit) (12,13). The H6-H8 chemical shift difference also provides a temperature sensitivity of 0.30±0.01 ppm/°C.

Interesting to note is that the temperature sensitivity can be cancelled if we choose two proton resonances with similar temperature sensitivities. For example, the chemical shift differences between H3 and H2 in Tm-DOTA-4AmP^{5-} provides a pH sensitivity of 0.37±0.02 ppm/pH unit and a temperature sensitivity of 0.054±0.001 ppm/°C (Figure 2, Table 1). This temperature sensitivity is 6 times smaller than that of the H6-H8 combination. Although the pH sensitivity for H3-H2 also decreases, this unique feature provides a possibility to determine pH from the chemical shifts while the temperature effect would be minimal. In Yb-DOTA-4AmP^{5-}, pH sensitivity can be enhanced to 2.1±0.1 ppm/pH unit when chemical shifts differences between proton resonances H1 and H8 are used. Meanwhile, this combination gives 0.130±0.002 ppm/°C in temperature sensitivity. Another combination of proton resonances (i.e., H5 and H4 in Yb-DOTA-4AmP^{5-}) shows high temperature sensitivity (0.89±0.01 ppm/°C) and relatively low pH sensitivity (0.35 ± 0.05 ppm/pH unit). Another advantage to use the chemical shift difference between two proton

resonances is to avoid errors caused by susceptibility, which can affect the frequency of water resonance. Although susceptibility effect on water protons does not give rise to large changes in shift (i.e., in the range of several Hz), it affects the water chemical shift measurements and thus temperature/pH determination. Because the chemical shifts of all proton resonances are normally referenced to water proton resonance, these experimental variations can be avoided when two independent signals are considered and their effects are cancelled out.

BIRDS properties of Tm-DOTA-4AmP^{5-} and Yb-DOTA-4AmP^{5-} show great sensing potential for pH and temperature. However pH and temperature measurements are interdependent through chemical shift changes. To determine pH and temperature simultaneously, two pairs of chemical shifts with different pH/temperature sensitivities are required. In this multi-parametric model, the pH and temperature were calculated from two chemical shift differences $\Delta\delta_1$ and $\Delta\delta_2$,

$$pH = A_1 + B_1 \cdot \Delta\delta_1 + C_1 \cdot \Delta\delta_2 + D_1 \cdot \Delta\delta_1^2 + E_1 \cdot \Delta\delta_2^2 + F_1 \cdot \Delta\delta_1 \cdot \Delta\delta_2 \quad (2)$$

$$T = A_2 + B_2 \cdot \Delta\delta_1 + C_2 \cdot \Delta\delta_2 + D_2 \cdot \Delta\delta_1^2 + E_2 \cdot \Delta\delta_2^2 + F_2 \cdot \Delta\delta_1 \cdot \Delta\delta_2 \quad (3)$$

where $\Delta\delta_1$ and $\Delta\delta_2$ are the chemical shift differences between two non-exchangeable protons on the probe and the coefficients A-F were determined from the fits (Table 2). For example, the chemical shift difference H6-H8 and H3-H2 in Tm-DOTA-4AmP^{5-} and H1-H8 and H5-H4 in Yb-DOTA-4AmP^{5-}, which represent $\Delta\delta_1$ and $\Delta\delta_2$ respectively for each probe, was used to determine T and pH (Supplementary Figure 3).

While BIRDS experiments detect non-exchangeable protons, exchangeable protons and/or bound water protons can be observed with CEST. At 35 °C and pH 7.5, the CEST effect of Yb-DOTA-4AmP^{5-} can be observed at about -18 ppm, whereas the CEST effect of Tm-DOTA-4AmP^{5-} can be observed at approximately -50 ppm, using 4 s saturation RF pulse with B_1 of 16.7 μT (Figure 3). The CEST peaks arise from the exchange between the amide protons and the bulk water protons. The CEST effects are not observed in TmDOTP^{5-} because it lacks exchangeable protons and bound water. In Figure 3, we demonstrate that the CEST effects are dependent on the pH and temperature for both complexes. Increasing pH results in increased CEST peak intensities but without significant shift of the peaks (less than 0.5ppm) for both complexes. Moreover, increasing the temperature, we observe an increase of CEST peak intensities but also a shift of the peak towards the water resonance in both complexes.

The CEST effect is usually quantified by CEST asymmetry as $1\text{-}M_s/M_0$, where M_s and M_0 are the values of water magnetization with and without RF saturation, respectively (Supplementary Figure 4). In 10 mM Yb-DOTA-4AmP^{5-} and 10 mM Tm-DOTA-4AmP^{5-}, the CEST effects at 35 °C increase linearly as pH increases from 6.3 to 7.9. The pH sensitivities of the CEST asymmetry ($1\text{-}M_s/M_0$) are 0.059±0.002 per pH unit and 0.034±0.002 per pH unit for Yb-DOTA-4AmP^{5-} and Tm-DOTA-4AmP^{5-}, respectively (Figure 4A). The temperature sensitivities of the CEST asymmetry are 0.012±0.001 per °C and 0.0073±0.0001 per °C for Yb-DOTA-4AmP^{5-} and Tm-DOTA-4AmP^{5-}, respectively

(Figure 4B). Note that in the pH range investigated (6.3 to 7.9), the CEST asymmetry (1-M_s/M_0) shows a linear pH dependence. However, in a similar CEST study (20), the authors reported a slightly non-linear pH dependence over this pH range. This could be due to different experimental conditions used in their study (a 20mM Yb-DOTA-4AmP^{5-} sample at 9.4 T, a temperature of 25°C and a saturation pulse of 11.7 μT for 4s) versus our study (a 10mM Yb-DOTA-4AmP^{5-} sample at 11.7 T, a temperature of 35°C, a saturation pulse of 16.7 μT for 4s). Different experimental conditions such as temperature or agent concentration could change the CEST asymmetry (1-M_s/M_0) and therefore result in a shift of the pH dependence such that it becomes linear over the pH range investigated in our study. For both pH and temperature, the sensitivities of the CEST asymmetry are higher in Yb-DOTA-4AmP^{5-} than those in Tm-DOTA-4AmP^{5-}. In addition, the chemical shift of the CEST peaks is also temperature sensitive but not pH sensitive. Therefore, the chemical shift of the CEST peaks can also be used for temperature determination, similar to BIRDS method (Supplementary Figure 5). The corresponding temperature sensitivities for the chemical shift of the CEST peaks are 0.34±0.01 ppm/°C and 0.13±0.02 ppm/°C for Yb-DOTA-4AmP^{5-} and Tm-DOTA-4AmP^{5-}, respectively. However, these temperature sensitivities are lower than those of non-exchangeable protons (Table 1). In addition, temperature mapping using the chemical shifts of the CEST peaks is not optimal because scanning of a relatively large number of frequencies (e.g. 10-20) is required to accurately measure the chemical shifts of the CEST peaks.

In vitro phantom studies of BIRDS imaging were performed on both Tm-DOTA-4AmP^{5-} and Yb-DOTA-4AmP^{5-} to demonstrate the generation of high-resolution pH and temperature maps with the proposed combination of protons (i.e., H6-H8 and H3-H2 for Tm-DOTA-4AmP^{5-}, and H1-H8 and H5-H4 for Yb-DOTA-4AmP^{5-}) (Figure 5). Two sets of phantoms were prepared for Tm-DOTA-4AmP^{5-} and Yb-DOTA-4AmP^{5-}, in each case three small adjacently placed glass tubes containing 10 mM solutions, but with different pH values: for Tm-DOTA-4AmP^{5-} at pH of 6.4, 7.2, and 7.8 from left to right and for Yb-DOTA-4AmP^{5-} at pH of 6.3, 7.1, and 7.8, from left to right (Figure 5). The pH values of these phantoms were independently measured with a pH electrode.

BIRDS experiments on Tm-DOTA-4AmP^{5-} and Yb-DOTA-4AmP^{5-} were acquired at 27.5 °C and 28.5 °C, respectively. The temperature values of these phantoms were independently confirmed with a thermocouple. To compensate the lower spatial resolution, we interpolated the BIRDS data to a matrix size of 128×128 (Figure 5 A-B, D-E) using a bicubic algorithm. Calculated temperature and pH distributions for each Tm-DOTA-4AmP^{5-} tube from left to right were 27.5±0.3, 27.7±0.3 and 27.4±0.4, and pH values were 6.43±0.03, 7.24 ±0.04, and 7.82±0.03 (Figure 5A and 5B). Calculated temperature and pH distributions for each Yb-DOTA-4AmP^{5-} tube from left to right were 28.4±0.1, 28.5±0.1 and 28.8±0.1, and pH values were 6.34±0.04, 7.10 ±0.02, and 7.80±0.04 (Figure 5D and 5E). The calculated values from BIRDS maps are in good agreement with the measured values, demonstrating the accuracy of the calibration obtained in Table 2 and Supplementary Figure 3.

CEST experiments were also acquired with the same phantoms. For Tm-DOTA-4AmP^{5-} at 27.5 °C, the CEST effects were 1.6±0.6%, 2.7±0.7%, and 4.1±1.2% for pH values of 6.4, 7.2, and 7.8, respectively (Figure 5C). For Yb-DOTA-4AmP^{5-} at 28.5 °C, the CEST effects

were 2.9±0.8%, 5.4±1.1%, and 9.6±1.5% for pH values of 6.3, 7.1, and 7.8, respectively (Figure 5F). The CEST effects in the imaging experiments were verified with CEST effects independently obtained from the Z-spectra (Supplementary Figure 6). Small deviations between two data sets in CEST experiments (imaging vs Z-spectrum) can be attributed to errors in estimation of saturation power and/or B1 inhomogeneities especially in the imaging experiments. As shown in Figure 5, for both Tm-DOTA-4AmP^{5-} and Yb-DOTA-4AmP^{5-}, the pH sensitivities are much higher in BIRDS than those in CEST, suggesting that BIRDS is more suitable for pH mapping with these agents. CEST experiments, however, can provide much higher spatial resolution. The improvement in spatial resolution in BIRDS is possible by designing new agents that contain more protons for detection or faster acquisition paradigms. A recent report has demonstrated that the effective voxel size of detection in BIRDS with other lanthanide agents can be reduced to 1 μL (22).

We believe that BIRDS and CEST can be used together to achieve high resolution pH imaging using either Tm-DOTA-4AmP^{5-} or Yb-DOTA-4AmP^{5-}. BIRDS provide both absolute temperature and pH maps with high sensitivities. More importantly, the temperature obtained from the BIRDS experiments can subsequently be used for determining saturation frequencies, which are temperature sensitive in the CEST experiments. The resulting images are pH-contrasted CEST effects (Figure 5C and 5D), as calibrated by BIRDS (Supplementary Figure 7). The calibration is a two-step process. First the absolute temperature from BIRDS is used to choose the optimal saturation offsets for each complex in the CEST experiment (Supplementary Fig. 5). Because there is a linear relationship between CEST effects in the imaging experiments and CEST effects from the Z-spectra (Supplementary Figure 6), choosing the right offset enables us to measure the other contributor to the CEST contrast (i.e., pH). Finally, the gray scale contrast for CEST is calibrated using the pH range established with BIRDS independently for each complex (Supplementary Figure 7). This calibration approach uses the higher molecular specificity of BIRDS with the higher spatial resolution of CEST for pH imaging.

Although Wolff and Balaban (14,15) showed that a change in the bulk water pool is observed when the pool of exchangeable protons is saturated with an RF pulse, the CEST contrast depends on a number factors which include the probe's ambient temperature and pH, the probe's concentration, and/or power of saturation RF pulse. Thus quantitative CEST measurements are difficult without careful estimation of the effects of all these factors. Herein, we believe quantitative BIRDS characterization of Tm-DOTA-4AmP^{5-} and Yb-DOTA-4AmP^{5-} can be used together with qualitative CEST experiments to provide a new detection scheme for molecular pH imaging, as was demonstrated recently with another PARACEST probe (11).

3. CONCLUSION

In summary, BIRDS and CEST studies of a phosphonate ligand (i.e., DOTA-4AmP^{5-}) chelated with two lanthanide metal ions (Tm^{3+} and Yb^{3+}) are described in this work. We showed that higher pH and temperature sensitivities are possible for BIRDS detection scheme when we use chemical shift differences between two proton resonances. In addition to the non-exchangeable protons for BIRDS detection, the exchangeable amide protons in

these two complexes can be observed in CEST experiments. The CEST effects observed together with BIRDS open up the possibility of high resolution quantitative pH imaging.

4. EXPERIMENTAL

4.1. Chemical synthesis

Tm-DOTA-4AmP^{5-} and Yb-DOTA-4AmP^{5-} were synthesized and prepared as previously reported (19,21). Briefly, diethyl bromoacetamidomethyl phosphonate was prepared from reaction between bromoacetyl bromide and diethyl aminomethyl phosphonate in presence of K_2CO_3 in benzene. Cyclen was alkylated by diethyl bromoacetamidomethyl phosphonate in presence of K_2CO_3 in acetonitrile to afford an ethyl ester of DOTA-4AmP^{5-}. The ethyl groups were removed by treating with 30% HBr in glacial acetic acid at room temperature to obtain DOTA-4AmP^{5-}. Finally, $LnCl_3$(Ln^{3+} = Tm^{3+}, Yb^{3+}) was incubated with DOTA-4AmP^{5-} at 60 °C for 12 hours to achieve the metal chelated complexes.

4.2. MR spectroscopy

The phantoms for BIRDS and CEST experiments were prepared by dissolving Tm-DOTA-4AmP^{5-} or Yb-DOTA-4AmP^{5-} complex in 90%/10% H_2O/D_2O (500 μL) at a concentration of 10 mM. The pH of the solution was adjusted using 10 mM phosphate buffer in the range 6.3-7.9. All MR experiments were performed using a vertical 11.7 T Bruker (Billerica, MA, USA) spectrometer.

4.3. BIRDS characterization

BIRDS characterization of Tm-DOTA-4AmP^{5-} and Yb-DOTA-4AmP^{5-} was assessed by measuring the chemical shifts of each resonance as a function of temperature with a series of phantoms containing samples at various pH values (6.3-7.9). pH and temperature dependencies of chemical shifts for proton resonances of Tm-DOTA-4AmP^{5-} and Yb-DOTA-4AmP^{5-} were fitted to a second-order polynomial equation (Eq.1) derived from multi-parametric data of chemical shift (δ), pH, and temperature (T) (12,13). pH and temperature were determined independently from two chemical shift differences using Eq.2 and Eq.3.

4.4. CEST characterization

CEST experiments of Tm-DOTA-4AmP^{5-} and Yb-DOTA-4AmP^{5-} were acquired by applying a 16.7 μT saturation pulse (4 s) followed by a 90° observe pulse to measure the intensity of the water signal (11). The ratio of water intensity (M_s/M_0) was plotted as a function of saturation frequency to obtain the Z spectrum. The CEST effect was quantified according to CEST%=$(1-M_s/M_0)\times100$.

4.5. In vitro BIRDS and CEST

Phantoms containing 10 mM Tm-DOTA-4AmP^{5-} of different pHs (i.e., pH 6.4, 7.2, and 7.8) and 10 mM Yb-DOTA-4AmP^{5-} of different pHs (i.e., pH 6.3, 7.1, and 7.8) were used for both BIRDS and CEST imaging. CSI and CEST data were obtained on a 11.7 T horizontal bore spectrometer using a surface coil RF probe (2 cm) and field of view of 20 × 20 mm. CSI experiments were acquired using 17×17 encoding steps, 128 averages, and TR

20 ms. A 204.8 μs SLR pulse was used for excitation. CEST images were acquired using a spin-echo imaging sequence with TR of 6 s, TE of 15 ms, and image matrix of 128×128. A 4 s continuous-wave of 16.7 μT was used for saturation at the frequencies of the exchangeable protons (saturation “on”) and at the frequencies on the opposite side from water (saturation “off”). The frequencies for the saturation were determined from Supplementary Figure. 4B, where the temperatures were determined from the BIRDS experiments. CEST contrast images representing the percent changes of image intensities were generated. The temperature was controlled by circulating constant-temperature hot air around the phantoms in the magnet bore and the temperature was monitored by thermocouple that was positioned close to the phantoms.

Supplementary Material

Refer to Web version on PubMed Central for supplementary material.

ACKNOWLEDGEMENTS

The authors thank the scientists and engineers at the Magnetic Resonance Research Center (MRRC) and Core center for Quantitative Neuroscience with Magnetic Resonance. This work was supported by grants from the National Institutes of Health (R01 CA-140102 to FH, R01 EB-011968to FH, P30 NS-052519 to FH, K25 CA-129173-04 to MA).

REFERENCES

1. Perez-Mayoral E, Negri V, Soler-Padros J, Cerdan S, Ballesteros P. Chemistry of paramagnetic and diamagnetic contrast agents for Magnetic Resonance Imaging and Spectroscopy pH responsive contrast agents. European journal of radiology. 2008; 67(3):453–458. [PubMed: 18455343]
2. Hashim AI, Zhang X, Wojtkowiak JW, Martinez GV, Gillies RJ. Imaging pH and metastasis. NMR in biomedicine. 2011; 24(6):582–591. [PubMed: 21387439]
3. Zhang X, Lin Y, Gillies RJ. Tumor pH and its measurement. Journal of nuclear medicine : official publication, Society of Nuclear Medicine. 2010; 51(8):1167–1170.
4. Zhang S, Wu K, Sherry AD. A Novel pH-Sensitive MRI Contrast Agent. Angew Chem Int Ed Engl. 1999; 38(21):3192–3194. [PubMed: 10556899]
5. Raghunand N, Howison C, Sherry AD, Zhang S, Gillies RJ. Renal and systemic pH imaging by contrast-enhanced MRI. Magnetic resonance in medicine : official journal of the Society of Magnetic Resonance in Medicine / Society of Magnetic Resonance in Medicine. 2003; 49(2):249–257.
6. Garcia-Martin ML, Martinez GV, Raghunand N, Sherry AD, Zhang S, Gillies RJ. High resolution pH(e) imaging of rat glioma using pH-dependent relaxivity. Magnetic resonance in medicine : official journal of the Society of Magnetic Resonance in Medicine / Society of Magnetic Resonance in Medicine. 2006; 55(2):309–315.
7. Bhujwalla ZM, McCoy CL, Glickson JD, Gillies RJ, Stubbs M. Estimations of intra- and extracellular volume and pH by 31P magnetic resonance spectroscopy: effect of therapy on RIF-1 tumours. British journal of cancer. 1998; 78(5):606–611. [PubMed: 9744499]
8. Ojugo AS, McSheehy PM, McIntyre DJ, McCoy C, Stubbs M, Leach MO, Judson IR, Griffiths JR. Measurement of the extracellular pH of solid tumours in mice by magnetic resonance spectroscopy: a comparison of exogenous (19)F and (31)P probes. NMR in biomedicine. 1999; 12(8):495–504. [PubMed: 10668042]
9. Garcia-Martin ML, Herigault G, Remy C, Farion R, Ballesteros P, Coles JA, Cerdan S, Ziegler A. Mapping extracellular pH in rat brain gliomas in vivo by 1H magnetic resonance spectroscopic imaging: comparison with maps of metabolites. Cancer research. 2001; 61(17):6524–6531. [PubMed: 11522650]

10. Gallagher FA, Kettunen MI, Day SE, Hu DE, Ardenkjaer-Larsen JH, Zandt R, Jensen PR, Karlsson M, Golman K, Lerche MH, Brindle KM. Magnetic resonance imaging of pH in vivo using hyperpolarized 13C-labelled bicarbonate. Nature. 2008; 453(7197):940–943. [PubMed: 18509335]
11. Coman D, Kiefer GE, Rothman DL, Sherry AD, Hyder F. A lanthanide complex with dual biosensing properties: CEST (chemical exchange saturation transfer) and BIRDS (biosensor imaging of redundant deviation in shifts) with europium DOTA-tetraglycinate. NMR in biomedicine. 2011; 24(10):1216–1225. [PubMed: 22020775]
12. Coman D, Trubel HK, Hyder F. Brain temperature by Biosensor Imaging of Redundant Deviation in Shifts (BIRDS): comparison between TmDOTP5- and TmDOTMA. NMR in biomedicine. 2010; 23(3):277–285. [PubMed: 19957287]
13. Coman D, Trubel HK, Rycyna RE, Hyder F. Brain temperature and pH measured by (1)H chemical shift imaging of a thulium agent. NMR in biomedicine. 2009; 22(2):229–239. [PubMed: 19130468]
14. Ward KM, Aletras AH, Balaban RS. A new class of contrast agents for MRI based on proton chemical exchange dependent saturation transfer (CEST). J Magn Reson. 2000; 143(1):79–87. [PubMed: 10698648]
15. Ward KM, Balaban RS. Determination of pH using water protons and chemical exchange dependent saturation transfer (CEST). Magnetic resonance in medicine : official journal of the Society of Magnetic Resonance in Medicine / Society of Magnetic Resonance in Medicine. 2000; 44(5):799–802.
16. Guivel-Scharen V, Sinnwell T, Wolff SD, Balaban RS. Detection of proton chemical exchange between metabolites and water in biological tissues. J Magn Reson. 1998; 133(1):36–45. [PubMed: 9654466]
17. Zhou J, Payen JF, Wilson DA, Traystman RJ, van Zijl PC. Using the amide proton signals of intracellular proteins and peptides to detect pH effects in MRI. Nature medicine. 2003; 9(8):1085–1090.
18. Aime S, Barge A, Delli Castelli D, Fedeli F, Mortillaro A, Nielsen FU, Terreno E. Paramagnetic lanthanide(III) complexes as pH-sensitive chemical exchange saturation transfer (CEST) contrast agents for MRI applications. Magnetic resonance in medicine : official journal of the Society of Magnetic Resonance in Medicine / Society of Magnetic Resonance in Medicine. 2002; 47(4):639–648.
19. Kalman FK, Woods M, Caravan P, Jurek P, Spiller M, Tircso G, Kiraly R, Brucher E, Sherry AD. Potentiometric and relaxometric properties of a gadolinium-based MRI contrast agent for sensing tissue pH. Inorganic chemistry. 2007; 46(13):5260–5270. [PubMed: 17539632]
20. Opina AC, Wu Y, Zhao P, Kiefer G, Sherry AD. The pH sensitivity of -NH exchange in LnDOTA-tetraamide complexes varies with amide substituent. Contrast media & molecular imaging. 2011; 6(6):459–464. [PubMed: 22144023]
21. Ali MM, Woods M, Caravan P, Opina AC, Spiller M, Fettinger JC, Sherry AD. Synthesis and relaxometric studies of a dendrimer-based pH-responsive MRI contrast agent. Chemistry. 2008; 14(24):7250–7258. [PubMed: 18601236]
22. Coman D, de Graaf RA, Rothman DL, Hyder F. In vivo three-dimensional molecular imaging with Biosensor Imaging of Redundant Deviation in Shifts (BIRDS) at high spatiotemporal resolution. NMR in biomedicine. 2013; 26(11):1589–1595. [PubMed: 23881869]
23. Robson MD, Gatehouse PD, Bydder M, Bydder GM. Magnetic resonance: an introduction to ultrashort TE (UTE) imaging. Journal of computer assisted tomography. 2003; 27(6):825–846. [PubMed: 14600447]
24. Gatehouse PD, Bydder GM. Magnetic resonance imaging of short T2 components in tissue. Clinical radiology. 2003; 58(1):1–19. [PubMed: 12565203]
25. Milne M, Hudson RH. Contrast agents possessing high temperature sensitivity. Chem Commun (Camb). 2011; 47(32):9194–9196. [PubMed: 21748170]
26. Hekmatyar SK, Poptani H, Babsky A, Leeper DB, Bansal N. Non-invasive magnetic resonance thermometry using thulium-1,4,7,10-tetraazacyclododecane-1,4,7,10-tetraacetate (TmDOTA(−)).

International journal of hyperthermia : the official journal of European Society for Hyperthermic Oncology, North American Hyperthermia Group. 2002; 18(3):165–179.

27. Zuo CS, Metz KR, Sun Y, Sherry AD. NMR temperature measurements using a paramagnetic lanthanide complex. J Magn Reson. 1998; 133(1):53–60. [PubMed: 9654468]

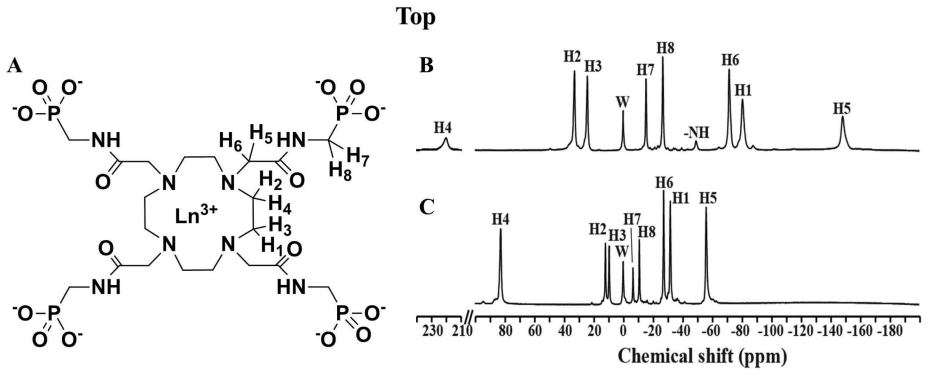

Figure 1.

Structure and proton spectra of lanthanide ions (Ln3+) chelated with DOTA-4AmP8-. (A) Chemical structure of DOTA-4AmP8- chelated with either thulium (Tm3+) or ytterbium (Yb3+). 1H MR spectra of 10 Mm solutions for (B) Tm-DOTA-4AmP5- and (C) Yb-DOTA-4AmP5- at 11.7 T at 35 °C and pH 7.4. W indicates water proton resonance, the different H's indicate the different non-exchangeable proton resonances for biosensor imaging of redundant deviation in shifts (BIRDS) and –NH represents the exchangeable proton resonances for chemical exchange of saturation transfer (CEST). Characterization of BIRDS and CEST for Ln- DOTA-4AmP5- are shown in Figures. 2 and 3 respectively.

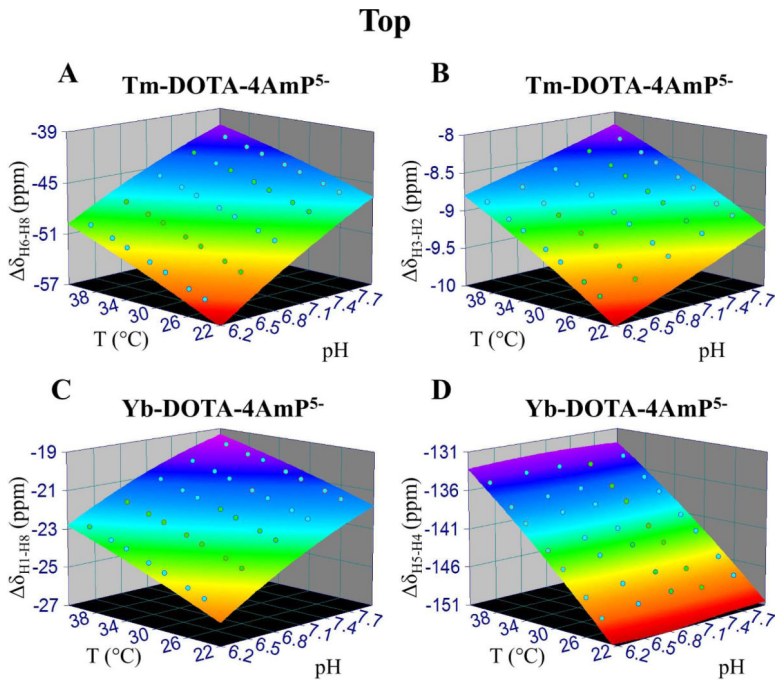

Figure 2.

BIRDS characterization. Temperature and pH dependencies of chemical shift differences between two non-exchangeable protons (A) H6 and H8 of Tm-DOTA-4AmP5-, (B) H3 and H2 of Tm-DOTA-4AmP5-, (C) H1 and H8 of Yb-DOTA-4AmP5-, and (D) H5 and H4 of Yb-DOTA-4AmP5-. Concentration of each complex was 10 mM. See Supplementary Figures 1 and 2 for temperature and pH dependent details on each nonexchangeable proton for Tm-DOTA-4AmP5- and Yb-DOTA-4AmP5-, respectively. Supplementary Figure 3 shows the other temperature and pH dependencies of chemical shift differences between two nonexchangeable protons. The temperature and pH sensitivities of each proton (determined with Eq. 1) and pairs of protons (determined with Eqs. 2 and 3) are shown in Table 1. The coefficients of Eq. 1 for Tm- DOTA-4AmP5- and Yb-DOTA-4AmP5- are shown Supplementary Tables 1 and 2, respectively. The coefficients of Eqs. 2 and 3 are shown in Table 2.

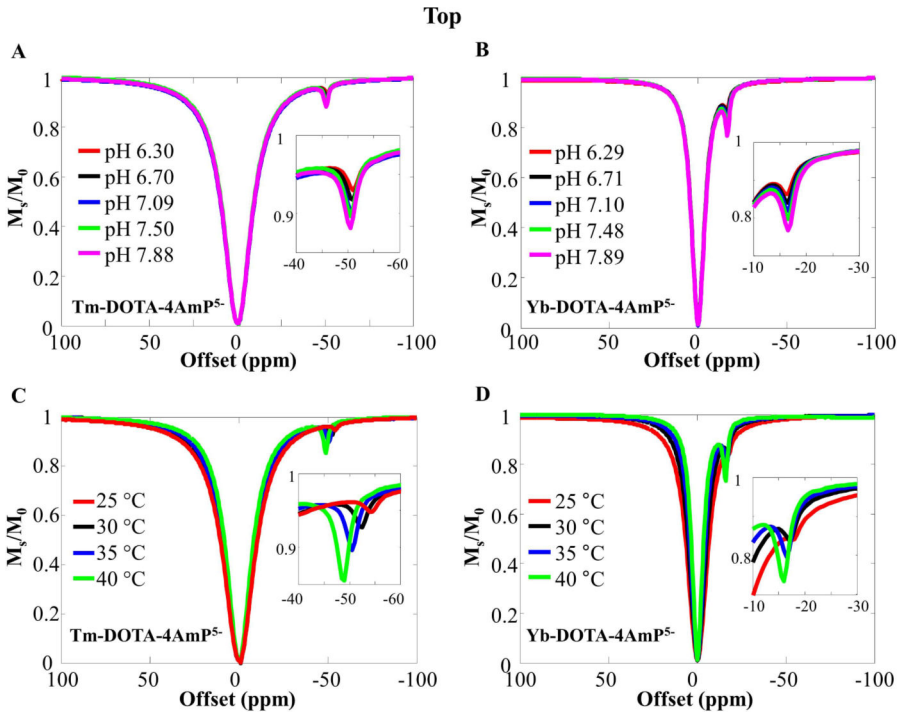

Figure 3.

CEST characterization . Z-spectra of samples containing 10 mM Tm-DOTA-4AmP5- and Yb-DOTA- 4AmP5-. The CEST effects of pH were recorded at 35 °C for (A) Tm-DOTA-4AmP5- and (B) Yb-DOTA-4AmP5-, while the CEST effects of temperature were recorded for (C) Tm-DOTA-4AmP5- at pH 7.50 and for (D) Yb- DOTA-4AmP5- at pH 7.48. Insets show magnified portions of the exchangeable proton pool. See Supplementary Figure 4 for the CEST asymmetry spectra.

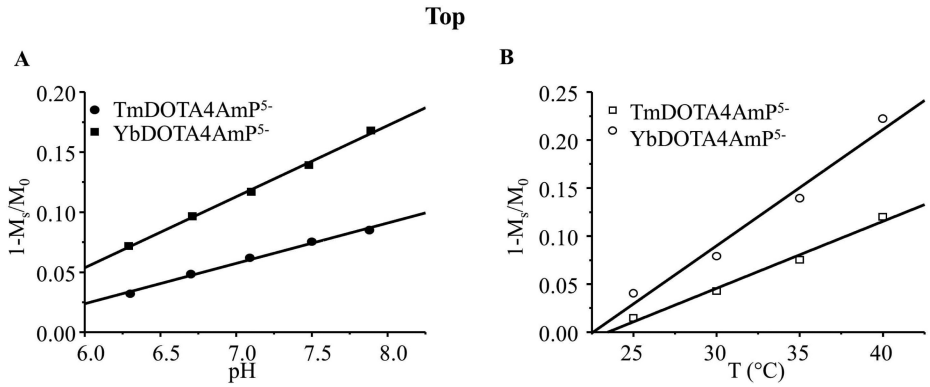

Figure 4.

The dependence of CEST effects of Tm-DOTA-4AmP5- and Yb-DOTA-4AmP5- on (A) pH in the range of 6.3 to 7.9 at 35 °C and (B) temperature in the range of 25 to 40 °C at pH 7.5. See Supplementary Fig. 5 for the saturation frequency offsets of the most intense CEST effect as a function of temperature for Ln- DOTA-4AmP5-.

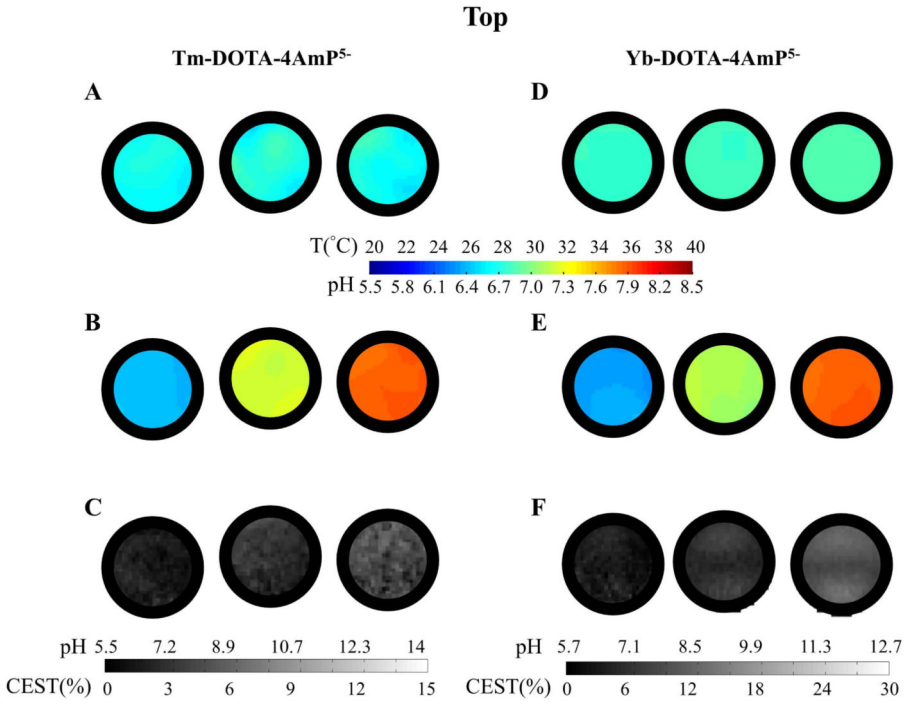

Figure 5.

BIRDS and CEST imaging studies for phantoms containing (A-C) Tm-DOTA-4AmP5- at different pH (i.e., pH 6.4, 7.2, and 7.8 from left to right), and (D-E) Yb-DOTA-4AmP5- at different pH (i.e., pH 6.3, 7.1, and 7.8 from left to right). Temperature mapping with BIRDS for both (A) Tm-DOTA-4AmP5- and (D) Yb- DOTA-4AmP5- shows homogeneous temperature distributions, while pH mapping with BIRDS for (B) Tm- DOTA-4AmP5- and (E) Yb-DOTA-4AmP5- shows accurate measurements of pH. CEST contrast generated for each phantom of (C) Tm-DOTA-4AmP5- and (F) Yb-DOTA-4AmP5- shows feasibility in pH mapping. BIRDS maps were interpolated to size of 128×128 to match the resolution of the CEST maps. The black circles represent the glass wall of the phantoms used for the experiments. The scale bar for A, B, D, and E represent temperature and pH from BIRDS, whereas the scale bar for C and F represent the calibrated gray scale for CEST depicting the pH range. The calibration is a two-step process: first, absolute temperature from BIRDS is used to choose the offset frequencies for CEST; second, the gray scale from CEST is calibrated according to pH range established by BIRDS. See text for details.

Table 1

BIRDS characterization of ^{1}H resonances in Tm-DOTA-4AmP^{5-} and Yb-DOTA-4AmP^{5-}

Resonance	Tm-DOTA-4AmP^{5-}		Yb-DOTA-4AmP^{5-}	
	pH sensitivity (ppm/pH unit)[a]	Temperature sensitivity (ppm/°C)[b]	pH sensitivity (ppm/pH unit)[a]	Temperature sensitivity (ppm/°C)[b]
H4	−3.9 ± 0.3	−1.49 ± 0.03	−0.62 ± 0.04	−0.52 ± 0.01
H2	−0.63 ± 0.04	−0.24 ± 0.01	−0.07 ± 0.01	−0.079 ± 0.001
H3	−0.25 ± 0.03	−0.188 ± 0.004	0.03 ± 0.01	−0.063 ± 0.001
H7	0.24 ± 0.04	0.121 ± 0.002	0.001 ± 0.001	0.051 ± 0.001
H8	−4.0 ± 0.2	0.170 ± 0.003	−1.68 ± 0.03	0.069 ± 0.001
H6	1.2 ± 0.1	0.47 ± 0.01	0.20 ± 0.02	0.17 ± 0.002
H1	1.8 ± 0.1	0.54 ± 0.01	0.38 ± 0.03	0.199 ± 0.002
H5	1.0 ± 0.1	1.04 ± 0.02	−0.27 ± 0.03	0.373 ± 0.004
H3-H2	0.37 ± 0.02	0.054 ± 0.001	-	-
H6-H8	5.2 ± 0.2	0.30 ± 0.01	-	-
H1-H8	-	-	2.1 ± 0.1	0.130 ± 0.002
H5-H4	-	-	0.35 ± 0.05	0.89 ± 0.01

[c] Measured at pH 7.48.

[a] Measured at 35 °C.

[b] Measured at pH 7.50.

Table 2

Coefficients for T and pH calculation using chemical shift differences of proton resonances in Tm-DOTA-4AmP^{5-} and Yb-DOTA-4AmP^{5-}

	A_1	B_1	C_1	D_1	E_1	F_1	r^2
$pH_{Tm\text{-}DOTA\text{-}4AmP5-}$	5.06	0.62	−3.61	0.017	0.29	−0.15	0.999
$pH_{Yb\text{-}DOTA\text{-}4AmP5-}$	8.16	0.98	−0.14	0.038	0.00042	−0.0083	0.999

	A_2	B_2	C_2	D_2	E_2	F_2	r^2
$T_{Tm\text{-}DOTA\text{-}4AmP5-}$	432.78	−5.38	98.8	−0.19	−0.67	1.66	0.999
$T_{Yb\text{-}DOTA\text{-}4AmP5-}$	381.00	1.55	3.59	0.13	0.011	−0.028	0.999